HHS Public Access

Author manuscript

Nat Commun. Author manuscript; available in PMC 2015 June 09.

Published in final edited form as:

Nat Commun. ; 5: 5662. doi:10.1038/ncomms6662.

Resolving Cancer-Stroma Interfacial Signaling and Interventions with Micropatterned Tumor-Stromal Assays

Keyue Shen[1], **Samantha Luk**[1], **Daniel F Hicks**[2], **Jessica S Elman**[1,5], **Stefan Bohr**[1,6], **Yoshiko Iwamoto**[3], **Ryan Murray**[1], **Kristen Pena**[4,7], **Fangjing Wang**[1,8], **Erkin Seker**[1,9], **Ralph Weissleder**[3], **Martin L Yarmush**[1], **Mehmet Toner**[1], **Dennis Sgroi**[2], and **Biju Parekkadan**[1,10]

[1]Department of Surgery, Center for Engineering in Medicine and Surgical Services, Massachusetts General Hospital, Harvard Medical School and the Shriners Hospitals for Children, Boston, Massachusetts 02114, USA

[2]Department of Pathology, Molecular Pathology Unit, Massachusetts General Hospital, Charlestown, Massachusetts 02129, USA

[3]Center for Systems Biology, Massachusetts General Hospital, Harvard Medical School, Boston, Massachusetts 02114, USA

[4]Department of Mechanical Engineering, Massachusetts Institute of Technology, Cambridge, Massachusetts 02139, USA

[10]Harvard Stem Cell Institute, Cambridge, Massachusetts 02138, USA

Abstract

Tumor-stromal interactions are a determining factor in cancer progression. *In vivo*, the interaction interface is associated with spatially-resolved distributions of cancer and stromal phenotypes. Here, we establish a micropatterned tumor-stromal assay (μTSA) with laser capture microdissection to control the location of co-cultured cells and analyze bulk and interfacial tumor-stromal signaling in driving cancer progression. μTSA reveals a spatial distribution of phenotypes in concordance with human estrogen receptor-positive (ER+) breast cancer samples, and

Correspondence should be addressed to: B.P. (biju_parekkadan@hms.harvard.edu) or K.S. (keyue.shen@usc.edu).
[5]Present address: Cell, Molecular & Developmental Biology Program, Tufts University, Boston, Massachusetts 02111, USA
[6]Present address: Department of Plastic Surgery, RWTH University Clinics, Aachen 52074, Germany
[7]Present address: Cor Medical Ventures, Solana Beach, California 92075, USA
[8]Present address: Allergan Inc., Irvine, California 92612, USA
[9]Present address: Department of Electrical and Computer Engineering, University of California, Davis, Davis, California 95616, USA

Competing Financial Interests

K.S. and B.P. are listed as inventors for a patent application disclosing μTSA, which includes data described in the manuscript.

Author Contributions

K.S. conceived and designed the study, performed all experiments, analyzed and interpreted data, and wrote the manuscript. J.S.E. performed cell culture, LCM, and animal study. D.F.H. performed LCM and animal study. S.B. contributed to primer designs and performed bioanalyzer electrophoresis. S.L. processed tissue and performed ex vivo luminescence study. Y.I. performed histological staining and Nanozoomer scanning. R.M. performed animal study and tissue processing. K.P. performed cell culture and stencil fabrication. F.W. contributed to ELISA and produced luicferase-reporter lentivirus. E.S. performed stencil fabrication. R.W., M.L.Y., M.T., and D.S. contributed to the concept and design of the study. M.L.Y. contributed to the funding of the study. D.S. analyzed and interpreted data. B.P. conceived and designed the study, provided funding, analyzed and interpreted data, and wrote the manuscript. All authors reviewed and revised the manuscript.

heterogeneous drug activity relative to the tumor-stroma interface. Specifically, an unknown mechanism of reversine is shown in targeting tumor-stromal interfacial interactions using ER+ MCF-7 breast cancer and bone marrow-derived stromal cells. Reversine suppresses MCF-7 tumor growth and bone metastasis *in vivo* by reducing tumor stromalization including collagen deposition and recruitment of activated stromal cells. This study advocates μTSA as a platform for studying tumor microenvironmental interactions and cancer field effects with applications in drug discovery and development.

Introduction

Epithelial cancer progression is associated with an evolving tissue interface of direct epithelial-stromal interactions[1]. In human tumor biopsies, extensive gene expression changes are correlated with cancer staging on both sides of the tumor-stroma interface[2, 3]; importantly, some epithelial-mesenchymal transition (EMT) signatures are preferentially expressed by cancer cells close to the interface, while interfacial stromal fibroblasts promote EMT more effectively than those extracted from the bulk millimeters away[4, 5]. It is however extremely difficult to clarify the exact, cell-specific contribution of tumor-stromal interactions in the development of this structure-function relationship in cancer progression *in vivo* because of a lack of experimental control[6]. Conventional *in vitro* models use random or transwell co-cultures to study contact- or soluble factor-mediated tumor-stromal signaling and screen for new drugs[7, 8]. However, in real tumors, cells at the tissue bulk and interface can be simultaneously and differentially influenced by the extent of heterotypic cell-cell contact and the long/short-range diffusion of soluble factors[9]. These models that indiscriminately mix two or more cell types cannot resolve this critical spatial perspective of tumor-stromal interactions, nor accurately assess drug action mechanisms in the heterogeneous cell compartments in the bulk and at the interface.

Micro-engineered cell cultures have emerged as powerful platforms to model processes in tissue microenvironments at appropriate length scales and identify their impact on cell morphogenesis and differentiation[10, 11, 12, 13]. Yet, the downstream analysis of micro-engineered cultures (as well as conventional cultures) has largely relied on resource-demanding immunocytochemistry, or mechanochemical cell isolation to understand cell-specific phenomena which introduces additional experimental artifacts and results in a loss of information on cells' original location. Microscopy-based laser capture has been used to retrieve cells in micropatterns for gene expression analysis[14]. However, the spatial resolution of the technique was not fully leveraged, and its combined use with micro-engineered cell co-cultures to understand spatially-defined signaling in cancer progression and drug actions has not been demonstrated to-date.

A micropatterned tumor-stromal assay (μTSA) is established to organize tumor and stromal cells into distinct, spatial compartments with a defined heterotypic cell interface. By integrating μTSA with microscopy and laser capture microdissection (LCM), we enable cell-specific analysis of phenotypes and gene expression *in situ* with precise spatial resolution. Using μTSA, we reveal a preferential instigation of malignant tumor-stromal signaling by bone marrow fibroblasts. Tumor cell expression profiles in μTSA are benchmarked against

human ER+ breast cancer tissue and found to have 63% concordance using a defined set of genes related to cancer progression. The co-culture system is further adapted to evaluate a new mechanism of action by known cancer therapeutics to disrupt tumor-stromal interfacial interactions with prediction of μTSA observations *in vivo*. Below, we present μTSA as a tool to explore a new frontier of tumor-stromal interfacial interactions with the underlying hypothesis that bulk and interfacial tumor cells can be differentially influenced by the type of neighboring stromal cell or a pharmacological intervention.

Results

Micropatterning to control a tumor-stroma interface

Micropatterned tumor-stromal assays (μTSAs) were designed to organize tumor and stromal cells into distinct, spatial compartments *in vitro* with a defined heterotypic cell interface by a stencil micropatterning technique[12, 15] (Fig. 1a), mimicking *in vivo* constraints on contact- and paracrine-signaling in the context of a growing tumor-stroma boundary layer. A cell-repellent, silicone mask was created with circular apertures that were cut by laser to form a cell culture stencil. The stencil mask defined the shape and size of areas where cancer cells initially attached and formed small multicellular islands (Fig. 1a). Stromal cells were seeded to occupy the rest of area after removal of the stencil, thereby creating a pre-determined tumor-stromal interaction interface (see **Methods**). Breast cancer and fibroblastic stromal cells were selected based on known stroma-induced tumor activity[16]. Figure 1b shows a μTSA of breast cancer cell MDA-MB-231 (engineered to express GFP[17]) and normal human dermal fibroblast (NHDF; stained for FSP-1) 24 hours after initial seeding. Notably, μTSA allows for seeding a fixed number of cancer and stromal cells while varying the total length of tumor-stromal interfaces (Supplementary Fig. 1). To demonstrate that an increased tumor-stromal interface would correlate with cancer-induced stromal function, MDA-MB-231 and NHDF were cultured in four representative seeding patterns in μTSA (Fig. 1c inset). Stromal secretion of IL-6[18] and CCL5[17], two tumor-inducing factors, increased as a function of tumor-stromal interfaces between MDA and NHDF cells, with a maximal found in random co-culture (Fig. 1c). The data suggest that the activation/sensitization of stroma by tumor cells is exquisitely controlled by direct contact.

Ki-67 evolves within μTSA under an inhibitory environment

NHDFs were previously reported to inhibit tumor cell proliferation[19]. μTSA was used to evaluate this purported anti-proliferative activity at the interface. Ki-67 in μTSA was measured as a proliferation marker in MDA-MB-231 cultures with or without NHDFs. Ki-67 remained predominantly expressed in MDA-MB-231 cells over time (Fig. 2a). Ki-67 intensity of individual cells was plotted against their radially-normalized location in the micropattern (Fig. 2b–c). MDA-MB-231 cells had significantly higher Ki-67 in mono-culture (Student's *t*-test, $p<0.01$) than in co-culture with NHDF (Fig. 2d). Interestingly, we saw an initial decrease in Ki-67 expression at day 2 in both conditions, followed by increased expression afterwards, suggesting a synchronization of cancer cell cycles when cultured in a micropatterned format (Fig. 2d). Ki-67 density in MDA-MB-231 mono-culture patterns showed a distinct spatial abundance in the periphery over time. In co-culture with NHDF, Ki-67 expression was static and revealed a spatial impact of NHDF on the

distribution of MDA-MB-231 proliferative activity (Fig. 2e). In agreement with the Ki-67 analysis, MDA-MB-231 cell number in μTSA was inhibited by surrounding NHDF cells (Fig. 2f). With the combined use of μTSA and transwell cell culture inserts, we designed a series of conditions that dissected individual elements in the NHDF inhibition, and found that both soluble factors and direct heterotypic cell-cell contact contributed to the inhibition (Supplementary Fig. 2).

LCM of μTSA uncover spatial phenotypic heterogeneity

LCM[20] was uniquely integrated with TSA to uncover cell-specific behavior *in situ* with precise spatial resolution. Cancer cells are proposed to coax the stromal microenvironment into a growth-promoting one by activating resident cells and/or recruiting bone marrow-derived cells[21, 22, 23], which in turn promote malignant phenotypes[22]. MCF-7, an estrogen-receptor positive breast cancer cell line, can metastasize to the bone marrow where bone marrow-derived mesenchymal stromal cells (BMSCs) reside; BMSCs, conversely, are recruited to primary lesions in MCF-7 xenograft tumor models[17]. μTSA co-culture of MCF-7 and BMSC illuminated a heterotypic interface (100~200 μm in width) highly positive for cytokeratins and vimentin, respectively (Fig. 3a). With LCM, we micro-dissected four regions of cells in μTSA defined by their proximity to the heterotypic interface and cell type (Fig. 3b). Micropattern design P2 (Fig. 1c **inset**) was selected for LCM studies because it provided optimal spatial resolution for distinguishing bulk and interfacial cells as well as cell capture/RNA extraction efficiency from these regions (Fig. 3c–d). The extracted RNA had an average RNA integrity number (RIN score) of 8.6 (standard deviation, SD=0.64) (Supplemental Fig. 3) out of a scale of 10 (intact RNA) to 1 (totally degraded RNA), which was suitable for gene expression analysis.

To reveal instigation of tumor-stromal signaling by stromal cells, expression of 11 cancer progression-related genes focusing on breast cancer cell invasion/migration and stroma activation (Supplementary Table 1) was compared in two breast cancer cell lines (MDA-MB-231, MCF-7) co-cultured with three relevant human fibroblastic stromal cells: (1) normal breast fibroblasts[24], (2) cancer-associated fibroblasts[24] and (3) BMSCs. BMSCs triggered the most frequent alteration of interfacial gene expression by both tumor cell lines (Fig. 3e), supporting a relatively stronger instigation of malignant phenotype by BMSCs. Comparative gene profiling between cells located at the interface vs. bulk areas in μTSA showed major differences in BMSC co-culture, where MCF-7 cells had a definitive, spatially-resolved gene expression pattern reflecting known *in vivo* observations (Fig. 3f). For example, *MMP14*[25], a metalloproteinase used for tumor cell invasion, and *TWIST1*[4, 26], an EMT marker indicative of migratory capability, were expressed higher by MCF-7 cells near a BMSC interface compared to bulk, suggesting promotion of cancer cell migration by BMSC through direct-contact or short-range, diffusible mediators. These data highlight the ability of a heterotypic tumor-stromal interface to induce localized phenotypic changes that promote malignant progression.

Human tumors have concordant spatial phenotypes with μTSA

LCM and spatial gene expression analysis were conducted on the 11-gene panel in five human breast cancer cases, to test whether the localized phenotypic differences relative to

the tumor-stromal interface in epithelial compartment observed in the μTSA mimic human patient conditions *in vivo*. Gene expression of epithelial cells adjacent to a tumor-stroma boundary (OE) was compared against those near the center (IE) in tumor nests with distinct morphological boundaries (Fig. 3g). A spatially regulated gene expression pattern emerged as a predominant feature in the epithelium of *in vivo* tumors (Fig. 3h). There was strong concordance with trends of gene expression observed in μTSA compared to the same genes measured in patient cases (Fig. 3i, 7 underlined genes out of 11 total, or 63.6%). A closer look at the magnitude of individual gene changes showed that *INHBA*, *TWIST1*, and *GREM1* were frequently up-regulated by ≥2-fold (60%, 80%, and 100% of the cases) in OE in the human tumors (Fig. 3h), which were all faithfully recapitulated by μTSA (Fig. 3f).

Spatially-resolved drug action is observed in μTSA

The μTSA/LCM system was further evolved to detect unknown, spatially-resolved mechanism of action by known cancer therapeutics to disrupt tumor-stromal interactions. In μTSA, we focused on disruption of progression-related tumor-stroma expression profile as an alternative to other forms of cancer drug efficacy (e.g. cytotoxicity). Using MCF-7 and BMSC mono-cultures, we pre-screened drugs known to: (1) target bone metastasis (zoledronate, pamidronate)[27], (2) interrupt stroma-induced tumor growth (reversine[8]), or (3) modulate BMSC signaling (bortezomib[28], indomethacin[29], aspirin[29], diphenhydramine[30]; rosiglitazone[31], resveratrol[32]). The top six drugs were selected according to their ability to maximally disrupt cancer signaling pathways in both cell types (Supplementary Table 2). μTSA of MCF-7 and BMSC were separately treated with the selected drugs (N=6 μTSAs per drug). LCM-captured cells were analyzed for gene expression and compared to the corresponding regions of μTSA without drug treatment (Fig. 4a). An aggregated metric, a μTSA gene expression score (see **Methods**), was introduced to compare drug effects in selective areas and μTSA as a whole. A negative score reflects a strong correlation to an expected inhibitory effect of a given drug against cancer.

Figure 4b depicts μTSA scores arranged in order of ‘best to worst’ with resolution of regional effects. Reversine stood out as the top candidate; importantly, reversine appeared to primarily affect gene expression at the tumor-stroma interface (Fig. 4c–d). Notably, reversine inhibited MCF-7 cell proliferation indicated by Ki-67 expression at the interface but not in the bulk. Though reversine has previously been reported to suppress the growth of multiple myeloma in the presence vs. the absence of BMSCs using an *in vitro* random co-culture[8], we found in a random co-culture experiment that, while MCF-7 growth was inhibited overall, no additional anti-proliferative effect by reversine was observed in mixed MCF-7/BMSC co-culture compared to MCF-7 monoculture (Supplementary Fig. 4). We further analyzed the gene expression change profile in both MCF-7 and BMSC in reversine-treated mixed MCF-7/BMSC co-culture compared to DMSO treatment by flow sorting (Supplementary Fig. 5). We observed a similar, attenuated profile in response to reversine treatment, as compared to that in the μTSA. In general, mixed co-culture represented an average of μTSA results. These data add to the notion that μTSA can identify drug mechanisms of action that target spatial/interfacial phenomena that are otherwise intractable in random co-cultures.

In vivo tumor growth is inhibited by reversine

We evaluated the activity of reversine on tumor-bearing mice to validate the relevance of μTSA indicated drug mechanisms targeting tumor-stroma interactions *in vivo*. MCF-7 cells engineered to express firefly luciferase (Luc) were used for *in vivo* tracking and measurement of organ metastases. We confirmed that luciferase tagging did not alter the MCF-7 phenotype, the response to stromal cells by transwell migration and invasion assays (no transmigration or invasion through membrane with 8 μm pore size, with or without matrigel), or gene expression (Supplementary Fig. 6). MCF-7/Luc cells were injected in the mammary fatpads using matrigel scaffolds in NOD/SCID mice. Tumor-bearing mice were either exposed to reversine or vehicle (DMSO). Tumor growth was monitored over an 8-week period, with an interim analysis at 4-weeks for histological and serological evaluation (Fig. 5a). We combined non-invasive and terminal approaches to accurately follow tumor burden. Caliper measurement evaluated the gross physical sizes of the tumors. Terminally-extracted tumors at week 4 and 8 were weighed, and biopsies of tumors were homogenized and measured for weight-adjusted luciferase activity *ex vivo* as a quantification of cancer cell-specific content. Tumor size, measured by caliper, was reduced in the reversine group after 21 days and beyond (Fig. 5b; Student's *t*-test, $p<0.05$). Measurement of tumor weights and *ex vivo* luciferase activity in tumor lysates confirmed that there were increases in tumor size in both treatment groups at week 8, and that a reduction in MCF-7 cancer cell number per tumor by reversine treatment, while insignificant at week 4, became significant at week 8 (Student's *t*-test, $p=0.002$, Fig. 5c). The primary tumor growth was thus largely unaffected by the reversine treatment until the late stages.

μTSA predicts reduction of tumor stromalization by reversine

We hypothesize that reversine could modify the stromal compartment of tumors based on modulation of tumor-stroma genes observed in μTSA and cause the late tumor growth inhibition. To test this hypothesis, tumor stromalization[33], defined here as the recruitment of stromal cells and deposition of extracellular matrix components, was quantified by histological metrics. In μTSA tests, *LOX1*, which is involved in collagen formation in tumors[34], was down-regulated in both epithelium and interfacial stroma (Fig. 3c–d). Collagen fibers facilitate tumor cell migration, stromal cell infiltration, and promote cancer cell growth[35]. In tumor sections rich of cancer cells, the collagen content in the DMSO group was significantly higher and more interspersed than that in the reversine group at week 4 and 8 (Fig. 6a–b, Student's *t*-test, $p=0.02$ and 0.003). *CXCL12*, a cytokine that drives the activation of local fibroblasts[24] and recruited BMSCs[36] into tumor-promoting myofibroblasts[16], was also found inhibited by reversine at the tumor-stroma interface in μTSA (Fig. 3c–d). ELISA analysis of tumor lysates showed a reduction of intratumoral CXCL12 level at week 8 in the reversine group (Supplementary Fig. 7, Student's *t*-test, $p=0.08$). Invasion and activation of stromal cells was examined by measuring the density of α-smooth muscle actin (α-SMA) positive cells in tumors. α-SMA is a marker for myofibroblasts which are promoted by CXCL12 signaling[24] and associated with invasive cancer growth and higher grade malignancy[16, 37]. The distribution of α-SMA+ cells was largely along the collagen-rich areas (Fig. 6c). The percentages of α-SMA+ cells in tumors

were different at week 8, but not week 4 (Fig. 6d), suggesting a dependence of α-SMA+ cell infiltration on the pre-formation of collagen network.

Decrease of metastases by reversine is bone marrow-specific

Metastasis, a watershed event in cancer progression[38, 39], represents an important endpoint in the study. Tumor metastatic potential is highlighted by *TWIST1*[40] and *COX2*[41, 42], which were both down-regulated in μTSA at the interface in epithelial and stromal cells, respectively (Fig. 3c–d). We harvested peripheral organs and measured luciferase activity in tissue lysates as an indicator of metastasis. Using a serial dilution of MCF-7/luc cells, we observed high linearity between luciferase activity in lysate versus cell numbers (Supplementary Fig. 8a). We determined that this method had a limit of detection (LOD) of 3 cells per mg tissue sample under our experimental settings, which was used as threshold value to detect the existence of micrometastases in both treatment groups at week 4 and 8. While no discernible metastases were found in week 4 groups, a number of organs were positively detected of cancer cells at the end of 8-week study in both groups (Supplementary Fig. 8b, summarized in Table 1), confirmed by immunohistochemical (IHC) staining of human mitochondria (Supplementary Fig. 9). Intriguingly, we detected no bone metastasis in any reversine-treated mice compared to 60% of mice in the DMSO group (Table 1). The blockade of bone metastasis was organ-specific, as cancer cells were detected in other organs at a similar frequency when comparing groups.

Discussion

The tumor-stromal interface is known to co-evolve with epithelial cancer from pre-invasive to malignant stages[43]. The mechanism of interfacial interactions in driving progression, and the implication for cancer therapeutics, are however largely unknown. To mimic the structurally constrained tumor-stromal interactions *in vivo*, we established μTSA as an enabling tool to probe tumor-stromal interfacial phenomena. Micropatterning allows for precise positioning of cell components according to their relative location in tumors, with simultaneous control over cell types, the number and ratio of cells, the degree of cell-cell interactions, and the accessibility of one cell to interact with another. The physical layout of cell-cell interactions on a two-dimensional surface integrates seamlessly with high-content microscopy imaging to allow for real-time and long-term monitoring of cell behaviors and signaling events with phenotypic markers and reporters. LCM was used for molecular profiling of cells in regions of interest to detect signaling changes in response to cell-cell interactions and drug interventions. The use of μTSA with other single-cell capture technologies including micromanipulators and optical trapping can also be envisioned for different applications.

In a μTSA model of MCF-7/BMSC, there was a boundary layer on the order of 1–10 cells in width with altered phenotypic expressions in cancer and stromal cells compared to the bulk areas (Fig. 3a). LCM and gene expression analysis revealed an array of signaling pathways that were differentially regulated at the interface vs. the bulk, particularly in the epithelial compartment. Notably, such localized, spatial phenotypic distributions were observed in human oral squamous cell carcinoma[44], and cervix and colon carcinomas[45] at similar length

scales. This underscores the structurally-/spatially-regulated interfacial signaling as a potential mechanism widely-applicable for the malignant transformation of the tumor microenvironments, as well as for the cancer field effect[46]. Future development of μTSA tumor models with various cancer and stromal types, and micropattern designs mimicking their physical parameters at different cancer stages will enable a systems-level revelation of interfacial signaling in a broad range of cancer types and stages. Conversely, an important application of the μTSA model will also be to validate and study the biological functions of oncogenes[47] and clinically discovered biomarkers[3].

Intratumor heterogeneity has important consequences in promoting tumor evolution and causing therapeutic failure[48]. A notable strength of the μTSA is thus in its ability to model the spatial phenotypic heterogeneity, and identify how drugs differentially modulate cells with regard to their location relative to an epithelial-stromal interface. For instance, reversine had markedly inhibitory effects in the interfacial cells compared to the bulk; resveratrol and bortezomib evenly influenced the different spatial regions; rosiglitazone had opposite overall impacts on epithelial and stromal compartments (Fig. 4b). Studying drug dose-response and combinatorial effects in μTSA will therefore contribute to the development of more effective therapeutic regimens. These applications demand high-throughput usage of μTSA either in direct functional read-out or downstream analyses. The current platform requires serial extraction of cells of interest with LCM equipment that limits operational efficiency and material yields. We were thus only able to analyze a limited number of genes at a time (Fig. 3e–f), or rely on amplification which introduces an additional complicated process prior to analysis. One adaptation of the platform will be to improve the engineering design of the co-culture substrate that can allow automated cell separation with high spatial accuracy[11], and the compatibility with current miniaturized assay platforms[49]. Another route is to combine the current μTSA/LCM techniques with high-throughput techniques such as RNA sequencing and gene expression microarrays, as well as systems biology approaches to discover pivotal molecular nodes in the tumor-stromal signaling. The identified targets will then allow the development of a small, but highly relevant array of reporters for drug screening readouts.

Different cancer types may follow distinct biological processes in the disease progression that correspond to different drug sensitivities[50]. The choice of gene targets (as well as stromal cells) thus should conform to the cancer model of interest, and will have significant impact on the drug discovery. In the present μTSA study, we chose a set of genes focusing on breast cancer cell invasion/migration and stroma activation. As a result, reversine was identified as a potential candidate to reduce the stromalization and bone metastasis in the chosen MCF-7/BMSC model. With established clinical reports on a plethora of gene expression signatures from human specimens[51, 52], the potential lists include, but are not limited to inflammation[53], angiogenesis, cell cycle, and metabolism[50]. Notably, another key aspect of the gene expression-based drug evaluation in μTSA is the aggregated gene expression score, where the weight scores were non-discriminatory for all the genes in the same category. This was for the consideration of nonlinear characteristic of signaling pathways (i.e. a specific expression change is not necessarily proportionally reflected in biological outcome)[54]. Until the quantitative contributions of targets are established, such

methodology remains practical, and one way to improve the robustness will be to expand the number of independent targets of interest.

Reversine is a synthetic purine that was originally discovered capable of dedifferentiating murine myoblasts to regain multipotency[55]. It has recently been found to possess antitumor capabilities, the exact mechanisms of which have not been clearly defined[8, 56, 57, 58, 59, 60, 61, 62]. The structural analogy of reversine to ATP implies its major function as a kinase inhibitor[8]. *In vitro*, reversine was found to suppress the expression of cell cycle related proteins MPS1, Aurora kinase A, B, and C, as well as cell growth signaling enzymes JAK2 and SRC[8, 57], and induce growth arrest, polyploidy, autophagy, and apoptosis[56, 58, 60]. *In vivo*, reversine was shown to mildly inhibit multiple myeloma growth in a mouse model with intravenous injection of tumor cells, but not with subcutaneous inoculation, indicating a role of the native bone marrow stromal environment in reversine-induced anti-myeloma activities[8]. Two more recent studies demonstrated that reversine inhibited subcutaneous human cervical and thyroid cancer cell growth in nude mouse models[61, 62]. Interestingly, both reports showed a mild, delayed tumor growth inhibition by reversine compared to DMSO treatments, with onsets of inhibition between 19 and 40 days after implantation, similar to the growth dynamics in the current study. However, both studies assumed a cancer cell-directed drug action without further *in vivo* analyses. The μTSA model suggests a novel drug mechanism by reversine on tumor stromalization and metastasis by targeting tumor-stromal interactions and is supported by our *in vivo* findings. The current data cannot completely rule out the contribution of direct inhibition of reversine on cancer cells. Future studies will be designed to separate it from the mechanisms targeting tumor-stromal interactions and stromalization. This can be potentially achieved by rescuing the major kinases affected by reversine in tumor cells, which is yet technically challenging due to the multiplicity of reversine targets[59].

It is important to clearly state that μTSA is not designed as an exact re-creation of *in vivo* tumors and can be improved upon further. In essence, it captures key tumor-stromal interactions in a spatially-regulated manner *in vitro* that mimics the biophysical constraints imposed by tumor morphology *in vivo*. In our study, we have used μTSA to explore a spatial heterogeneity of gene expression patterns that was validated by comparison to patient tumor tissue samples. Value in the assay was further gained by its application in drug testing and the new perspective on drug action mechanisms with predictive power to *in vivo* pre-clinical endpoints. A more comprehensive gene expression study in μTSA with reference to more human cases can strengthen the statistic confidence in our concordance level (~63%) and greatly expand targets that can be explored in μTSA. A further improvement of μTSA to model human cancer will be the extension of this model from 2-D to 3-D. There have been reports showing that some cell signaling and phenotypes in the *in vivo* tumor environments only occur in 3-D cultures[63, 64]. Additionally, the diffusion of soluble factors, the effect of extended cell shape with associated rearrangements of the cytoskeleton and intercellular connections, and the sensitivity to anticancer drugs can be very different between 2-D and 3-D environments[65, 66]. One of the future directions will be to incorporate 3-D elements such as matrix embedment and physical constraints on diffusion, while retaining the ability to interface with microscopy-based and/or high-throughput techniques. While doing so, it will

be important to observe if genes that were different between μTSA and human tumor samples *in vivo* (e.g. *MMP11*) revert to similar trends or remain discordant before further follow-up.

In summary, μTSA uniquely recapitulates the epithelial-stromal invasion front in tumor microenvironments with extensive control over various microenvironmental parameters. μTSA, coupled with LCM, allowed for direct analyses of phenotypic and gene expression changes in a spatially-resolved manner. Heterotypic cell-cell interactions were explored across multiple tumor-stroma pairs to optimize the model. We also demonstrated the translational application of μTSA in discovering a new mechanism of chemotherapeutic drugs that target tumor-stromal interactions. A μTSA-selected drug, reversine, was explored for *in vivo* efficacy and suppressed tumor growth and bone metastasis through reduced stromal activation in agreement with *in vitro* μTSA test observations. This technology is flexible, scalable, and poised to synergize with the ever-growing field of pharmacogenomics as a platform for diagnostic and therapeutic discovery at the tumor-stroma interface.

Methods

Cells

MDA-MB-231 expressing green fluorescent protein (GFP) was a generous gift from Weinberg lab[17]. Normal breast fibroblast (NBF) and cancer-associated fibroblast (CAF) were provided by Orimo lab and previously described by Kojima et al.[24] MCF-7 and normal human dermal fibroblast (NHDF) were purchased from ATCC. For *in vivo* studies, MCF-7 cells were engineered to express firefly luciferase with a lentivirus containing luciferase reporter (MCF-7/Luc) following a previous report[67]. Primary human bone marrow mesenchymal stromal/stem cells (BMSCs) were derived from whole human bone marrow aspirates (Lonza)[68]. BMSCs were expanded in alpha-modified Minimum Essential Medium Eagle (alpha-MEM), 20 mg L^{-1} gentamycin, 10% FBS, 2.5 ug L^{-1} rhFGF-basic (R&D Systems), 100 U ml^{-1} penicillin, and 100 mg ml^{-1} streptomycin. All other cells and co-cultures were grown in Dulbecco's MEM (DMEM) supplemented with 10% FBS, 100 U ml^{-1} penicillin and 100 μg ml^{-1} streptomycin.

Antibodies

Antibodies used for staining included: anti-pan-cytokeratin (clone C11, 1:500) and vimentin (clone D21H3, 1:200) (Cell Signaling), anti- α-smooth muscle actin (α-SMA) (clone 1A4, 1:200) (Dako), anti-Ki-67 (rabbit polyclonal, ab15580, 1:300) (Abcam), anti-CD105-PE (clone SN6, 1:100) (eBioscience), anti-mitochondria (clone 113-1, 1:100) and anti-fibroblast specific protein-1 (FSP-1; rabbit polyclonal, 07-2274, 1:200) (Millipore). IL-6 ELISA kit was purchased from BD Biosciences. CCL5 DuoSet ELISA kit and mouse CXCL12/SDF-1 alpha Quantikine ELISA Kit were from R&D Systems. Alexa Fluor® fluorescent dye-conjugated secondary antibodies were from Life Technologies for immunofluorescent staining.

Reagents

Aspirin, indomethacin, resveratrol, reversine, rosiglitazone, and zoledronic acid were purchased from Sigma-Aldrich. Bortezomib was from LC Laboratories. Pamidronate and diphenhydramine were from Massachusetts General Hospital (MGH) Pharmacy. Duration of drug treatment *in vitro* was 48 hours for all drugs. Concentrations used for drug treatment on the mono-culture and co-cultures are based on the half maximal effective concentrations (EC_{50}) of the selected drugs: aspirin: 10 μM (for COX-2 inhibition); bortezomib: 20 nM; diphenhydramine: 10 μM; indomethacin: 40 μM; pamidronate: 20 μM; resveratrol: 20 μM; reversine: 5 μM; rosiglitazone: 100 nM; zoledronic acid: 40 μM.

Micropatterned tumor stromal assay and drug treatment

Round glass coverslips (12 mm in diameter, Fisher Scientific) were cleaned by immersion into hot detergent (MP Biomedicals 7X, diluted 1:3 with deionized water), rinsed with deionized water, and dried with nitrogen gas. The cleaned coverslips were treated with oxygen plasma (PDC-32G, Harrick Plasma) for 5 minutes, and silanized for 15 minutes with 1% N-(2-aminoethyl)-3-aminopropyl-trimethoxy-silane (Sigma) diluted in deionized water immediately before the treatment. The coverslips were then extensively rinsed in deionized water, dried with nitrogen gas, and cured at 100 °C for 1 hour. Lab prepared rat tail collagen I[69] was diluted 1 mg/ml in 0.1% acetic acid and coated onto glass coverslips overnight, which were then air-dried and sterilized by UV exposure for 10 min. Stencils were made by cutting circular features of a series of diameters with a laser engraver (Zing Technologies) in a 250 μm-thick silicone sheet (Rogers Corporation). The stencils were then thoroughly rinsed in 70% ethanol and deionized water, and air dried in sterile environment. Stencils were applied onto coated glass coverslips, and the whole substrate were submerged in 0.2% (w/v) Pluronic F-127 (Sigma) in PBS for 1 hour, and rinsed 3 times in PBS. Substrates were seeded with cancer cells at a density of 1.5×10^5 cells cm^{-2}, incubated for 1 hour, and rinsed in warm media. After overnight incubation, stencils were removed and the glass coverslips with micropatterned cancer cell areas were rinsed again with warm media and seeded with stromal fibroblastic cells at 2×10^4 cells cm^{-2}, incubated for 30 min and thoroughly rinsed to remove cells landed on the cancer islands. In drug treatment experiments, drugs were applied on μTSA 24 hours after the addition of stromal cell, and extended for 48 hours.

Ki-67 positivity analysis in μTSA

To quantitatively analyze Ki-67 in the spatial and temporal dimensions, the intensity of Ki-67 staining in individual cells was registered against their locations in the micropattern island (defined as normalized distance of the cells from the center of the area by the furthest cell in the same direction, r/r_{max}, Fig. 1e). The positivity was determined by thresholding the intensity against the staining of the surrounding non-proliferative stromal cells, and the whole circular region was divided into two categorical areas – a central area ($r/r_{max}<0.5$) and an outer annular area ($r/r_{max}>0.5$) representing the proximity to the border. The density of Ki-67 in each area was defined as total number of Ki-67 positive cells divided by total cell numbers in that area (determined by nucleus staining).

Laser capture microdissection

μTSA co-cultures of MCF-7 and MSC samples were rinsed twice with PBS, fixed with 70% ethanol, rinsed with deionized water, and stained with hematoxylin and eosin (H&E). All aqueous solutions were treated with diethylpyrocarbonate (DEPC) to avoid RNA degradation. The samples were then submerged in xylene, and air-dried immediately before being mounted with cell side up on glass slides for microdissection. Cells of interest were captured using a PixCell Iie LCM system (Arcturus Engineering). A cell-capturing cap with a special thermoplastic film was put in contact with μTSA surface, and locally melted into cells of interest in vicinity by low energy infrared laser pulses after microscopic visual selection. When the cap was released from the μTSA surface, it brought cells of interest on the film for subsequent RNA extraction processes.

RNA extraction and quantitative PCR

RNA was extracted with QIAGEN Rneasy Plus Micro kit, and the quality was evaluated by Agilent 2100 Bioanalyzer (Santa Clara, CA). RNA samples were reverse-transcribed and amplified with QIAGEN QuantiTect Whole Transcriptome kit into cDNA following manufacturer's protocol. Real-time quantitative PCRs were conducted with ViiA™ 7 system (Applied Biosystems). PCR reagents were obtained from QIAGEN. Primers were designed using NCBI Primer-BLAST and synthesized at MGH DNA Core Facility. Primer sequences are as listed in Supplementary Table 3.

LCM and gene expression analysis of clinical specimens

Five ER+ breast tumor specimens were obtained from the Massachusetts General Hospital, which were all formalin-fixed paraffin-embedded (FFPE) biopsies. Three of the tissue specimens were classified as invasive ductal carcinoma (IDC), and the rest two were ductal carcinoma *in situ* (DCIS). LCM were performed in the tumor nest areas with clear morphological boundaries between epithelial and stromal compartments. For each specimen, a total of 10 7-μm tissue sections were microdissected, and RNA was extracted and purified with Arcturus® Paradise® PLUS FFPE RNA Isolation Kit (Life Technologies) following the manufacturer's protocol. The purified RNA samples were then reverse transcribed (SuperScript® VILO™ cDNA Synthesis Kit, Life Technologies), pre-amplified (TaqMan® PreAmp, Life Technologies), and analyzed for the expressions of housekeeping genes and the 11 genes of interest with TaqMan® Gene Expression Assays (Supplementary Table 4, Life Technologies). The conduct of this work was covered by an approval from the Massachusetts General Hospital Institutional Review Board, and written informed consent was obtained from all the subjects.

μTSA gene expression scoring

The expression change of each gene (designated as i) was scored as expression score E_i with −1 (down-regulated by ≥2-fold), 0 (between −1 and 1), or 1 (up-regulated by ≥2-fold). Based on the biological functions and clinical associations with cancer progression, each gene was also assigned with a weight score W_i of −1 (inhibitory or negatively associated with progression), 0 (no or complex association, or redundant with other genes in the list), or 1 (cancer-promoting or positively associated with progression) (Supplementary Table 5).

Multiplying the direction of expression change (E_i) with its weight (W_i) indicates the functional impact of a given drug on a specific molecular target, and the sum total score provides an overall evaluation ($\Sigma E_i \, xW_i$).

Gene expression analysis of random MCF-7 and BMSC coculture

To keep cell number/ratio and culture format the same as μTSA, MCF-7 and BMSC were admixed at the ratio of 1:3 and seeded in 24-well plate at 10,000 MCF-7 and 30,000 BMSC per well. Cells were co-cultured without drugs for 24 hours, treated with DMSO or reversine (5 M) for 48 hours, trypsinized, pooled, stained for CD105-PE, and sorted for the positive (BMSC) and negative (MCF-7) fractions on a Modified Digital Vantage Cell Sorter at the MGH Flow Cytometry Core Facility. The sorted cells were extracted for RNA with QIAGEN Rneasy Plus Micro kit. RNA was reverse transcribed with SuperScript® VILO™ cDNA Synthesis Kit (LifeTechnologies), and real-time quantitative PCRs were conducted with ViiA™ 7 system (Applied Biosystems) using primer sequences listed in Supplementary Table 3.

Treatment and measurement of MCF-7 xenograft tumor model

6-week old *NOD.CB17-Prkdcscid/J* female mice were purchased from Jackson Laboratory and maintained in the animal facility at MGH. Experiments were approved by and conducted in accordance with the policies of the Institutional Animal Care and Use Committee of MGH. Mice were implanted subcutaneously behind neck with estrogen pellets (17 β-estradiol, 0.72 mg per pellet, 60-day release, Innovative Research of America). MCF-7 cells expressing luciferase were resuspended in phosphate buffered saline (PBS) and 1:1 mixed with high-concentration matrigel (BD Bioscience) and injected in the two abdominal mammary fat pads (1×10^7 cells per site in 100 μl volume). 20 animals were evenly assigned into two groups (n=10 for both DMSO group and reversine group) and subjected to treatments twice a week. Reversine stock solution in DMSO was diluted in saline and injected intraperitoneally (i.p.) in the treatment group at a dose of 0.5 mg per kilogram body weight. Control group was treated i.p. with the same dose of DMSO carrier diluted in saline. Tumors were allowed to growth for 4 to 8 weeks, with half of the population (n=5 from each group) sacrificed at week 4 and the other half at week 8. Tumor sizes was measured in the following ways: (1) caliper measurement of the two perpendicular (longest/shortest) axes in the x/y plane, with tumor volume calculated as $\pi xy^2/6$ assuming an ellipsoidal shape, (2) ex vivo bioluminescence measurement of luciferase activity per weight of tumor biopsy (1/4 tumors cut along the long and short axes) lysate, and total signal per tumor back-calculated with tumor weights. At week 4 and 8, lung, liver, kidney, spleen and hind leg bone from sacrificed animals were snap-frozen in liquid nitrogen for *ex vivo* luciferase activity assay. Tumors were extracted and cut in halves, with half snap-frozen for luciferase activity assay and the other half fixed in 10% formalin, dehydrated in 70% ethanol, and processed for standard immunohistochemical analyses.

Detection of metastases by ex vivo luciferase activity assay

Tissues of interest were individually pulverized into a fine powder by hand grinding with a dry ice-chilled porcelain mortar and pestle, and transferred to 1.5 ml tubes on dry ice.

Grinded tissues were weighted and added with Promega Reporter Lysis Buffer, vortexed for 15 min, frozen and thawed three times with alternating liquid nitrogen and 37 °C water bath, and centrifuged at 12,000 x g. 20 μl of each supernatant was mixed with 100 μl of Luciferase Assay Reagent (Promega) and measured for luminescence in a non-transparent white plate (Corning) by BioTek Synergy 2 plate reader. The luciferase activity in lysate was shown to have a wide linear range with regard to cell numbers by a two-fold dilution series of a known-number of MCF-7/Luc cells (Supplementary Fig. 8a). The positivity of metastases was determined by Limit of Detection (LOD) calculated with formula[70]: $LOD=mean_{blank} + 1.635(SD_{blank}) + 1.635(SD_{low\ concentration\ sample})$, where $mean_{blank}$ and SD_{blank} are the mean and standard deviation of the replicates of a blank sample, and $SD_{low\ concentration\ sample}$ is the standard deviation of the replicates of the sample containing the lowest concentration of the cell lysate.

Immunohistochemistry

Fixed tumor samples were processed, embedded in paraffin, and sectioned in 5 μm thickness by Specialized Histopathology Services at MGH. Tissue sections were stained with H&E, Masson's trichrome, and antibodies against α-SMA. Images were scanned by Nanozoomer 2.0RS (Hamamatsu Japan). Collagen density was calculated as the proportion of blue collagen staining in each field of view in the Masson's trichrome staining. α-SMA density was evaluated similarly by the percentage area covered by α-SMA positive cells in each field of view.

Statistical analysis

All data are presented in mean ± standard deviation (SD), as stated in the figure legends. Statistical significance was assessed using Student's *t*-test for pair-wise comparison and gene expression, χ^2 test for non-parametric comparison, and 1-way ANOVA for comparison between multiple (≥3) conditions; $p<0.05$ was considered as significant.

Supplementary Material

Refer to Web version on PubMed Central for supplementary material.

Acknowledgments

We thank Dr. Robert A. Weinberg for the MDA-MB-231/GFP cells; Dr. Akira Orimo for the normal breast fibroblasts and cancer associated fibroblasts; Daniel Datorre and Drs. Jack M. Milwid and William McCarty for assistance with animal work; Patricia Della Pelle and Anna Levitz for assistance with histology. This work was supported in part by the Shriners Hospitals for Children (B.P), National Institutes of Health Grants R01EB012521 (B.P.) and K01DK087770 (B.P.), and also by Massachusetts General Hospital Fund for Medical Discovery (K.S.).

References

1. Sgroi DC. Preinvasive breast cancer. Annu Rev Pathol. 2010; 5:193–221. [PubMed: 19824828]
2. Allinen M, et al. Molecular characterization of the tumor microenvironment in breast cancer. Cancer Cell. 2004; 6:17–32. [PubMed: 15261139]
3. Ma XJ, Dahiya S, Richardson E, Erlander M, Sgroi DC. Gene expression profiling of the tumor microenvironment during breast cancer progression. Breast Cancer Res. 2009; 11:R7. [PubMed: 19187537]

4. De Wever O, et al. Molecular and pathological signatures of epithelial – mesenchymal transitions at the cancer invasion front. Histochem Cell Biol. 2008; 130:481–494. [PubMed: 18648847]
5. Gao MQ, et al. Stromal fibroblasts from the interface zone of human breast carcinomas induce an epithelial-mesenchymal transition-like state in breast cancer cells in vitro. J Cell Sci. 2010; 123:3507–3514. [PubMed: 20841377]
6. Polyak K, Hu M. Do myoepithelial cells hold the key for breast tumor progression? J Mammary Gland Biol Neoplasia. 2005; 10:231–247. [PubMed: 16807803]
7. Casbas-Hernandez P, Fleming JM, Troester MA. Gene expression analysis of in vitro cocultures to study interactions between breast epithelium and stroma. J Biomed Biotechnol. 2011; 2011:520987. [PubMed: 22203785]
8. McMillin DW, et al. Tumor cell-specific bioluminescence platform to identify stroma-induced changes to anticancer drug activity. Nat Med. 2010; 16:483–489. [PubMed: 20228816]
9. Shvartsman SY, Wiley HS, Deen WM, Lauffenburger DA. Spatial Range of Autocrine Signaling: Modeling and Computational Analysis. Biophys J. 2001; 81:1854–1867. [PubMed: 11566760]
10. Nelson CM, et al. Emergent patterns of growth controlled by multicellular form and mechanics. Proc Natl Acad Sci U S A. 2005; 102:11594–11599. [PubMed: 16049098]
11. Hui EE, Bhatia SN. Micromechanical control of cell-cell interactions. Proc Natl Acad Sci U S A. 2007; 104:5722–5726. [PubMed: 17389399]
12. Bhatia SN, Balis UJ, Yarmush ML, Toner M. Microfabrication of hepatocyte/fibroblast co-cultures: role of homotypic cell interactions. Biotechnol Prog. 1998; 14:378–387. [PubMed: 9622518]
13. El-Ali J, Sorger PK, Jensen KF. Cells on chips. Nature. 2006; 442:403–411. [PubMed: 16871208]
14. Lee JY, Jones C, Zern MA, Revzin A. Analysis of local tissue-specific gene expression in cellular micropatterns. Anal Chem. 2006; 78:8305–8312. [PubMed: 17165820]
15. Folch A, Toner M. Microengineering of cellular interactions. Annual review of biomedical engineering. 2000; 2:227–256.
16. Orimo A, et al. Stromal fibroblasts present in invasive human breast carcinomas promote tumor growth and angiogenesis through elevated SDF-1/CXCL12 secretion. Cell. 2005; 121:335–348. [PubMed: 15882617]
17. Karnoub AE, et al. Mesenchymal stem cells within tumour stroma promote breast cancer metastasis. Nature. 2007; 449:557–563. [PubMed: 17914389]
18. Knupfer H, Preiss R. Significance of interleukin-6 (IL-6) in breast cancer (review). Breast Cancer Res Treat. 2007; 102:129–135. [PubMed: 16927176]
19. Flaberg E, et al. High-throughput live-cell imaging reveals differential inhibition of tumor cell proliferation by human fibroblasts. Int J Cancer. 2011; 128:2793–2802. [PubMed: 20715102]
20. DeCarlo, K.; Emley, A.; Dadzie, O.; Mahalingam, M. Laser Capture Microdissection: Methods and Applications. In: Murray, GI., editor. Laser Capture Microdissection. Humana Press; 2011.
21. Mueller MM, Fusenig NE. Friends or foes - bipolar effects of the tumour stroma in cancer. Nat Rev Cancer. 2004; 4:839–849. [PubMed: 15516957]
22. Bissell MJ, Hines WC. Why don’t we get more cancer? A proposed role of the microenvironment in restraining cancer progression. Nat Med. 2011; 17:320–329. [PubMed: 21383745]
23. Bissell MJ, Radisky D. Putting tumours in context. Nat Rev Cancer. 2001; 1:46–54. [PubMed: 11900251]
24. Kojima Y, et al. Autocrine TGF-beta and stromal cell-derived factor-1 (SDF-1) signaling drives the evolution of tumor-promoting mammary stromal myofibroblasts. Proc Natl Acad Sci U S A. 2010; 107:20009–20014. [PubMed: 21041659]
25. Friedl P, Alexander S. Cancer Invasion and the Microenvironment: Plasticity and Reciprocity. Cell. 2011; 147:992–1009. [PubMed: 22118458]
26. Soini Y, et al. Transcription factors zeb1, twist and snai1 in breast carcinoma. BMC Cancer. 2011; 11:1–8.
27. Palmieri C, Fullarton JR, Brown J. Comparative efficacy of bisphosphonates in metastatic breast and prostate cancer and multiple myeloma: a mixed-treatment meta-analysis. Clin Cancer Res. 2013

28. Wang X, Zhang Z, Yao C. Bortezomib Inhibits the Angiogenesis Mediated by Mesenchymal Stem Cells. Cancer Invest. 2012; 30:657–662. [PubMed: 23013101]
29. Singh-Ranger G, Salhab M, Mokbel K. The role of cyclooxygenase-2 in breast cancer: review. Breast Cancer Res Treat. 2008; 109:189–198. [PubMed: 17624587]
30. Nemeth K, et al. Characterization and function of histamine receptors in human bone marrow stromal cells. Stem Cells. 2012; 30:222–231. [PubMed: 22045589]
31. Takada I, Kouzmenko AP, Kato S. PPAR-gamma signaling crosstalk in mesenchymal stem cells. PPAR Research. 2010; 2010
32. Peltz L, et al. Resveratrol Exerts Dosage and Duration Dependent Effect on Human Mesenchymal Stem Cell Development. PLoS One. 2012; 7:e37162. [PubMed: 22615926]
33. Gupta PB, et al. Systemic Stromal Effects of Estrogen Promote the Growth of Estrogen Receptor – Negative Cancers. Cancer Res. 2007; 67:2062–2071. [PubMed: 17332335]
34. Csiszar K. Lysyl oxidases: a novel multifunctional amine oxidase family. Prog Nucleic Acid Res Mol Biol. 2001; 70:1–32. [PubMed: 11642359]
35. Provenzano P, et al. Collagen density promotes mammary tumor initiation and progression. BMC Med. 2008; 6:11. [PubMed: 18442412]
36. Direkze NC, et al. Bone marrow contribution to tumor-associated myofibroblasts and fibroblasts. Cancer Res. 2004; 64:8492–8495. [PubMed: 15574751]
37. Sappino AP, Skalli O, Jackson B, Schurch W, Gabbiani G. Smooth-muscle differentiation in stromal cells of malignant and non-malignant breast tissues. Int J Cancer. 1988; 41:707–712. [PubMed: 2835323]
38. Sgroi DC. Breast cancer Src activity: bad to the bone. Cancer Cell. 2009; 16:1–2. [PubMed: 19573804]
39. Hanahan D, Weinberg RA. Hallmarks of cancer: the next generation. Cell. 2011; 144:646–674. [PubMed: 21376230]
40. Kalluri R, Weinberg RA. The basics of epithelial-mesenchymal transition. J Clin Invest. 2009; 119:1420–1428. [PubMed: 19487818]
41. Hu M, Peluffo G, Chen H, Gelman R, Schnitt S, Polyak K. Role of COX-2 in epithelial-stromal cell interactions and progression of ductal carcinoma in situ of the breast. Proc Natl Acad Sci U S A. 2009; 106:3372–3377. [PubMed: 19218449]
42. Nakagawa H, et al. Role of cancer-associated stromal fibroblasts in metastatic colon cancer to the liver and their expression profiles. Oncogene. 2004; 23:7366–7377. [PubMed: 15326482]
43. Hansen RK, Bissell MJ. Tissue architecture and breast cancer: the role of extracellular matrix and steroid hormones. Endocr Relat Cancer. 2000; 7:95–113. [PubMed: 10903527]
44. Vidal M, et al. A Role for the Epithelial Microenvironment at Tumor Boundaries: Evidence from Drosophila and Human Squamous Cell Carcinomas. The American Journal of Pathology. 2010; 176:3007–3014. [PubMed: 20363916]
45. Franci C, et al. Expression of Snail protein in tumor-stroma interface. Oncogene. 2006; 25:5134–5144. [PubMed: 16568079]
46. Chai H, Brown RE. Field Effect in Cancer – An Update. Ann Clin Lab Sci. 2009; 39:331–337. [PubMed: 19880759]
47. Leung CT, Brugge JS. Outgrowth of single oncogene-expressing cells from suppressive epithelial environments. Nature. 2012; 482:410–413. [PubMed: 22318515]
48. Gerlinger M, et al. Intratumor Heterogeneity and Branched Evolution Revealed by Multiregion Sequencing. N Engl J Med. 2012; 366:883–892. [PubMed: 22397650]
49. Khetani SR, Bhatia SN. Microscale culture of human liver cells for drug development. Nat Biotechnol. 2008; 26:120–126. [PubMed: 18026090]
50. Garnett MJ, et al. Systematic identification of genomic markers of drug sensitivity in cancer cells. Nature. 2012; 483:570–575. [PubMed: 22460902]
51. Lapointe J, et al. Gene expression profiling identifies clinically relevant subtypes of prostate cancer. Proc Natl Acad Sci U S A. 2004; 101:811–816. [PubMed: 14711987]
52. Perou CM, et al. Molecular portraits of human breast tumours. Nature. 2000; 406:747–752. [PubMed: 10963602]

53. Chang HY, et al. Robustness, scalability, and integration of a wound-response gene expression signature in predicting breast cancer survival. Proc Natl Acad Sci U S A. 2005; 102:3738–3743. [PubMed: 15701700]
54. Downward J. The ins and outs of signalling. Nature. 2001; 411:759–762. [PubMed: 11459043]
55. Chen S, Zhang Q, Wu X, Schultz PG, Ding S. Dedifferentiation of Lineage-Committed Cells by a Small Molecule. J Am Chem Soc. 2003; 126:410–411. [PubMed: 14719906]
56. Hsieh TC, Traganos F, Darzynkiewicz Z, Wu JM. The 2,6-disubstituted purine reversine induces growth arrest and polyploidy in human cancer cells. Int J Oncol. 2007; 31:1293–1300. [PubMed: 17982654]
57. D'Alise AM, et al. Reversine, a novel Aurora kinases inhibitor, inhibits colony formation of human acute myeloid leukemia cells. Mol Cancer Ther. 2008; 7:1140–1149. [PubMed: 18483302]
58. Kuo CH, et al. Reversine induces cell cycle arrest, polyploidy, and apoptosis in human breast cancer cells. Breast Cancer. 2012
59. Jemaa M, et al. Preferential killing of p53-deficient cancer cells by reversine. Cell Cycle. 2012; 11:2149–2158. [PubMed: 22592527]
60. Lee YR, et al. Reversine suppresses oral squamous cell carcinoma via cell cycle arrest and concomitantly apoptosis and autophagy. J Biomed Sci. 2012; 19:9. [PubMed: 22283874]
61. Hua S-C, et al. Reversine, a 2,6-disubstituted Purine, as an Anti-cancer Agent in Differentiated and Undifferentiated Thyroid Cancer Cells. Pharm Res. 2012; 29:1990–2005. [PubMed: 22477067]
62. Qin HX, et al. Synergistic antitumor activity of reversine combined with aspirin in cervical carcinoma in vitro and in vivo. Cytotechnology. 2013
63. Wang F, et al. Reciprocal interactions between β1-integrin and epidermal growth factor receptor in three-dimensional basement membrane breast cultures: A different perspective in epithelial biology. Proceedings of the National Academy of Sciences. 1998; 95:14821–14826.
64. Debnath J, Brugge JS. Modelling glandular epithelial cancers in three-dimensional cultures. Nat Rev Cancer. 2005; 5:675–688. [PubMed: 16148884]
65. Pampaloni F, Reynaud EG, Stelzer EHK. The third dimension bridges the gap between cell culture and live tissue. Nat Rev Mol Cell Biol. 2007; 8:839–845. [PubMed: 17684528]
66. Friedrich J, Seidel C, Ebner R, Kunz-Schughart LA. Spheroid-based drug screen: considerations and practical approach. Nat Protoc. 2009; 4:309–324. [PubMed: 19214182]
67. Love Z, et al. Imaging of mesenchymal stem cell transplant by bioluminescence and PET. J Nucl Med. 2007; 48:2011–2020. [PubMed: 18006616]
68. Parekkadan B, et al. Mesenchymal stem cell-derived molecules reverse fulminant hepatic failure. PLoS One. 2007; 2:e941. [PubMed: 17895982]
69. Silver FH, Trelstad RL. Type I collagen in solution. Structure and properties of fibril fragments. J Biol Chem. 1980; 255:9427–9433. [PubMed: 7410433]
70. Armbruster DA, Pry T. Limit of blank, limit of detection and limit of quantitation. Clin Biochem Rev. 2008; 29 (Suppl 1):S49–52. [PubMed: 18852857]

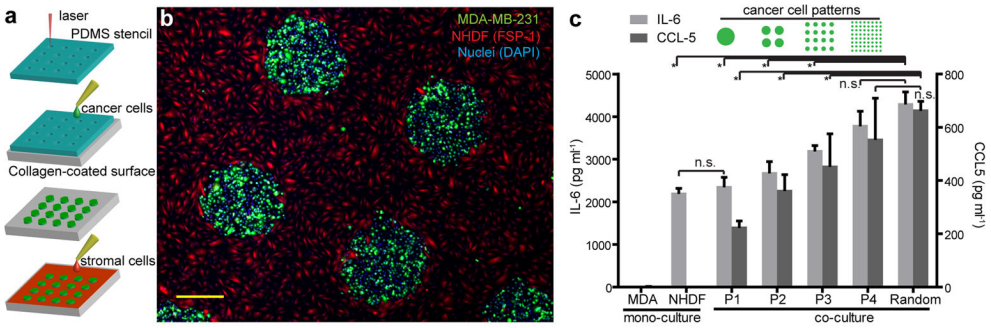

Figure 1. Heterotypic cell-cell interactions are precisely controlled in micropatterned tumor stromal assay (μTSA)

(a) Schematics of the μTSA fabrication process. (b) μTSA co-culture of MDA-MB-231 (expressing GFP) breast cancer cell with normal human dermal fibroblasts (NHDF) (stained for fibroblast-specific protein-1, FSP-1). Scale bars: 100 μm. (c) 48-hour IL-6 and CCL5 secretion in MDA and NHDF mono-cultures, random and μTSA co-cultures with 4 different micropattern designs. n.s.: not significant; *: $p<0.05$, by one-way ANOVA. (c) n=3. Error bars: standard deviation (SD).

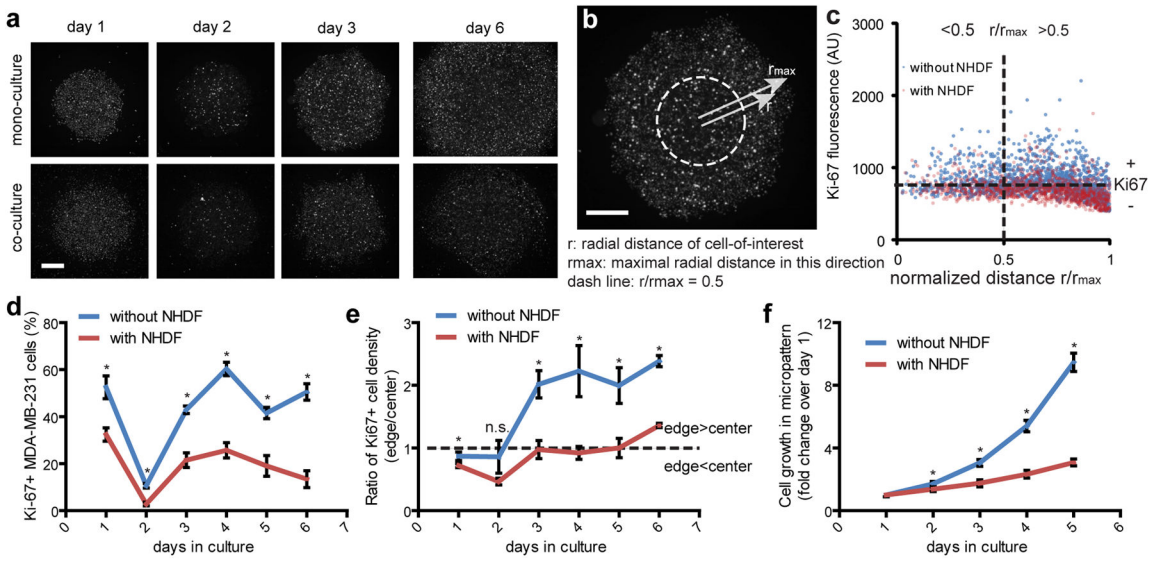

Figure 2. Ki-67 expression in MDA-MB-231 cells is spatially regulated and inhibited by NHDF cells in micropatterned cultures

(a) Images of Ki-67 staining in MDA mono-culture and co-culture with NHDF over 6 days. (b) Image analysis of Ki-67 positivity in μTSA. r: radial distance r of a cancer cell from the center of micropattern; r_{max} center-to-edge distance along the same vector direction; dash line: r/r_{max}=0.5 separates cancer cell region into central and edge areas (see **Methods**). (c) Cellular Ki-67 staining intensities were plotted against normalized distances, and threshold into positive and negative cells. (d) Percentage of Ki-67+ MDA cells in micropatterns in absence (blue) and presence (red) of surrounding NHDF cells over 6 days. (e) The ratio of the Ki-67+ MDA cell density between micropattern edge (area outside dash line) and center (area within dash line). (f) MDA cell growth in micropatterns without or with NHDF cells, measured by total GFP intensity in each micropattern area. Scale bars: 500 μm. (d~f) n.s.: not significant; *: $p<0.05$ by Student's *t*-test. (d~e) n=3 per condition per day; (f) n=6 per condition. Error bars: SD.

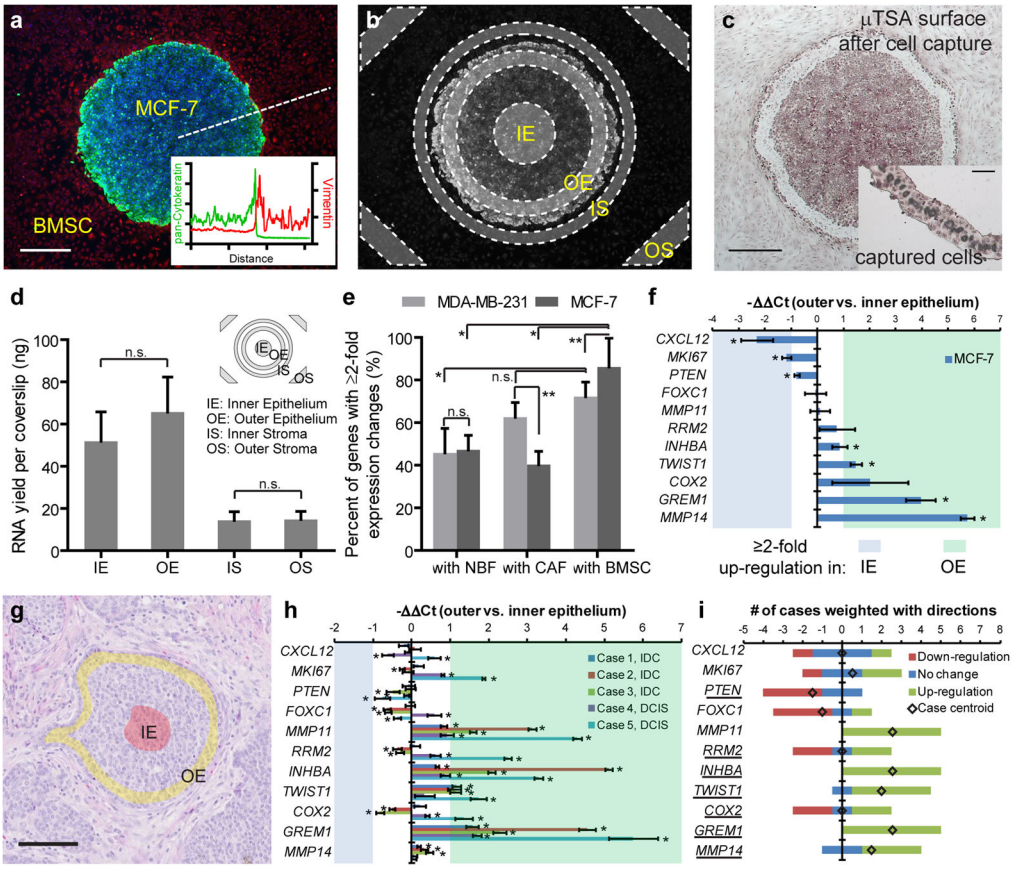

Figure 3. Laser capture microdissection (LCM) uncovers spatial phenotypic heterogeneity in μTSA and concordance in human breast cancer tissue

(a) μTSA co-culture of MCF-7 (green: pan-cytokeratin) and bone marrow derived mesenchymal stromal cell (BMSC; red: vimentin). Nuclei were counterstained with DAPI (blue). Inset: line scan of green and red channels from the center of micropattern into the bulk of BMSC. Scale bar: 500 μm. (b) Four categorical cell regions IE, OE, IS, and OS in μTSA (locations: **I**nner and **O**uter; cell components: **E**pithelium and **S**troma) (c) A μTSA co-culture of MCF-7 and BMSC cells after LCM capture of interfacial cancer cells (H&E). Inset: Captured cells on a thermoplastic membrane. Scale bars: 500 μm and 100 μm (inset). (d) Average ribonucleic acid (RNA) yield from four regions of a single 4-island μTSA co-culture. n.s.: not significant by Student *t*-test. (e) Percent of genes with ≥2-fold expression change in MCF-7 cells out of the 11 genes examined when co-cultured with normal breast fibroblast (NBF), cancer-associated fibroblast (CAF) and BMSC in μTSA. n.s.: not significant; *: $p<0.05$, by one-way ANOVA; **: $p<0.05$, by Student's *t*-test. (f) Relative gene expression change in interface vs. bulk in cancer cells. (g) Clinical specimen of human breast cancer (a case of IDC) and bulk (IE) & interfacial (OE) regions used for LCM and gene expression analysis. Scale bar: 100 μm. (h) Relative expression (−ΔΔ Ct) of the 11 genes in OE versus IE were plotted in the same way as (f). (i) Direction-weighted, stacked numbers of cases for each gene with significant ($p<0.05$) up- or down-regulations, or no change ($p \geq 0.05$). Centroids (diamond) indicate overall direction of gene expression by simple case majority in up- and down-regulations. Underlined genes (7 out of 11, or 63.6%)

have matched directions (including no change by p-value) in μTSA. (f, h) *: $p<0.05$ by Student's *t*-test, samples had significant changes in gene expression; all other conditions: no significance in gene expression change. (d) n=5~6; (e) n=6; (f, h) n=3. (d~f, h) Error bars: SD.

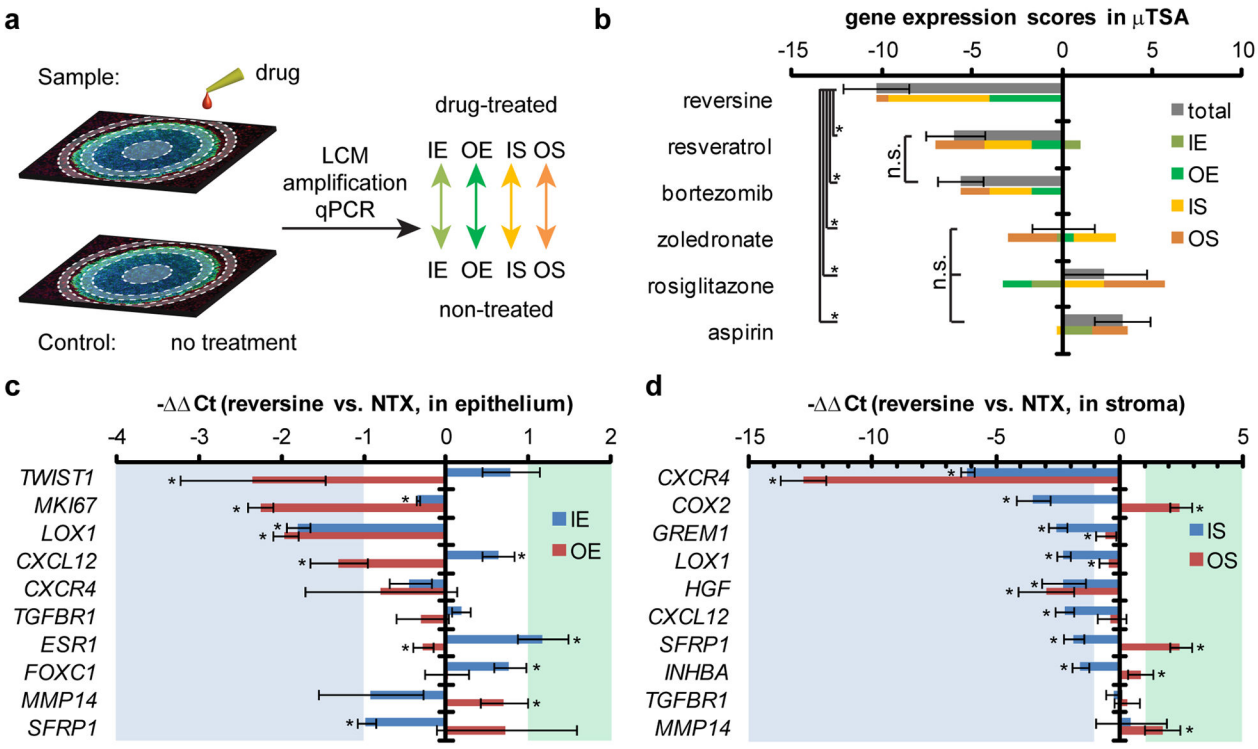

Figure 4. Reversine is selected in spatially-resolved μTSA drug test with gene expression as readout

(a) Gene expressions in IE, OE, IS and OS were compared between drug treated and non-treated co-cultures of MCF-7 and BMSC in μTSA. (b) A collection of six drugs were tested on the μTSA platform and the scores sorted from negative (cancer-inhibiting) to positive (cancer-promoting), where reversine stood out as the top candidate. Scores from individual regions were plotted in color bars. n.s.: not significant between the indicated groups; *: $p<0.05$, by one-way ANOVA. Gene expression changes in (c) IE and OE and (d) IS and OS caused by reversine treatment. *: $p<0.05$ by Student's *t*-test, samples had significant changes in gene expression; all other conditions: no significance in gene expression change. (b~d) n=6. Error bars: SD.

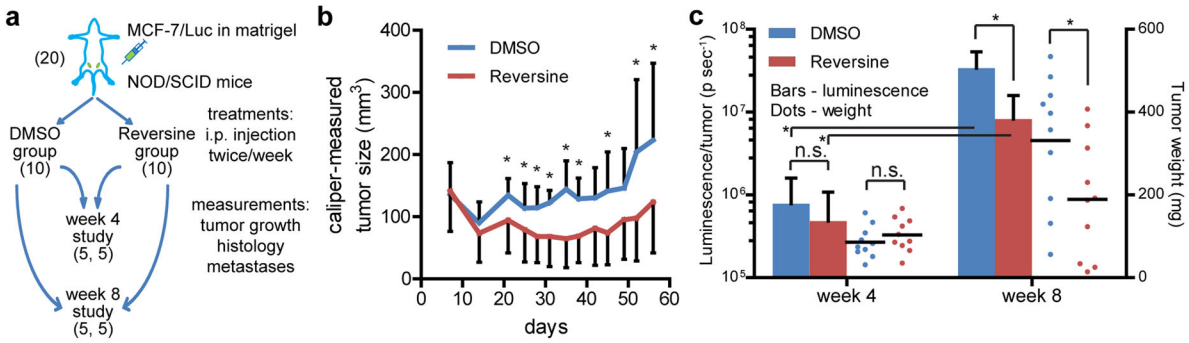

Figure 5. Reversine treatment inhibits in vivo tumor growth in a MCF-7 tumor model

(a) MCF-7 cells expressing luciferase were implanted in NOD/SCID mammary fatpads in a total of 20 mice, and monitored for tumor growth with (N=10) and without (N=10) reversine treatment. (b) Tumor growth by caliper measurements. *: $p<0.05$ by Student's *t*-test; all others: not significant. (c) *ex vivo* bioluminescent signal and tumor weights measured from extracted tumors at week 4 and 8 (N=5 from each group, respectively). n.s.: not significant; *: $p<0.05$ by Student's *t*-test. (b~c) Error bars: SD.

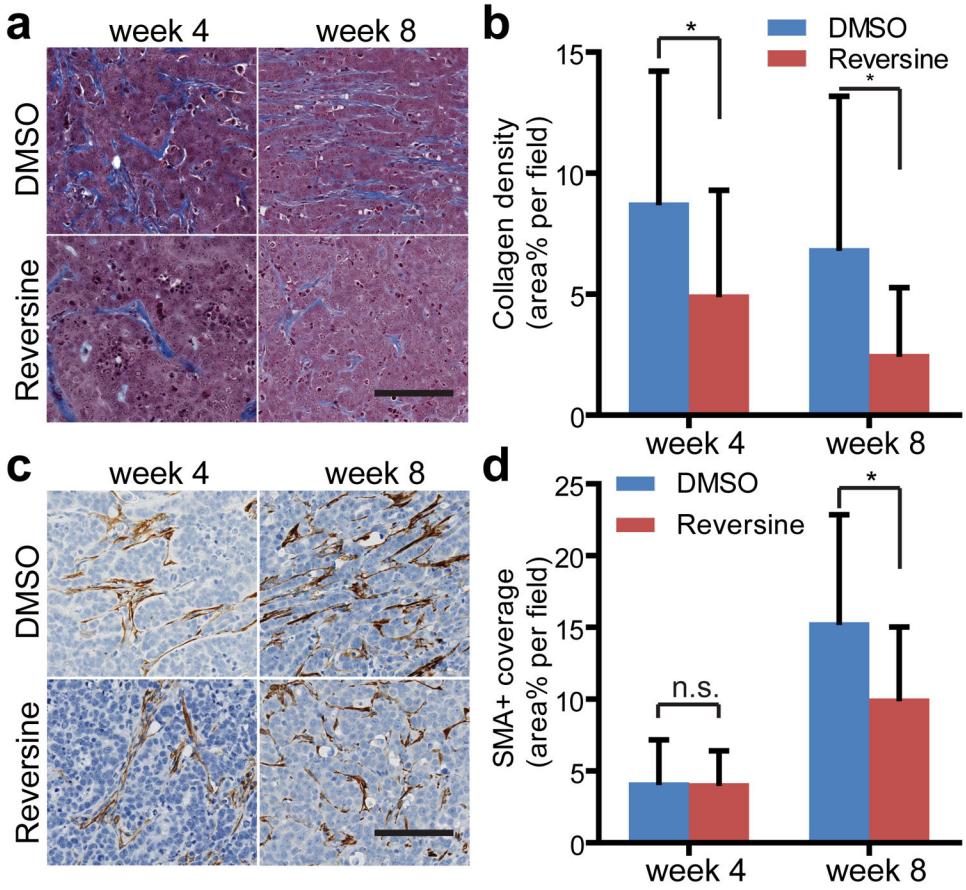

Figure 6. Tumor stromalization is reduced by reversine treatment

(a) Masson's trichrome staining, (b) quantification of collagen density, (c) immunohistochemical α-smooth muscle actin (αSMA) staining, and (d) percentage of areas occupied by αSMA+ cells in each field of view. Evaluations were made in tumor areas dominated by cancer cells at week 4 and 8 in the control and reversine treatment groups. Images were taken at 20x magnification representing 5 tumors per group. Image numbers analyzed (week 4 DMSO, week 4 Reversine, week 8 DMSO, week 8 Reversine): n=21, 22, 27, and 24 for collagen density; n=35, 55, 129, and 92 for SMA. (a, c) Scale bars: 100 μm. (b, d) Error bars: SD. n.s.: not significant; *: $p<0.05$ by Student's *t*-test.

Table 1

Reversine treatment leads to bone marrow-specific reduction of metastases detected at week 8

distal sites	DMSO (affected animals/group size)	Reversine (affected animals/group size)	p-value (χ^2)
lung	0/5	1/5	0.2918
liver	1/5	1/5	1
spleen	1/5	1/5	1
kidney	2/5	1/5	0.4902
bone	3/5	0/5	0.0384